MATERIALS CHEMISTRY
FRONTIERS

RESEARCH ARTICLE

View Article Online
View Journal | View Issue

Cite this: *Mater. Chem. Front.*, 2019, **3**, 1779

Optimization of oxygen evolution dynamics on RuO_2 *via* controlling of spontaneous dissociation equilibrium†

Yu Sun,[a] Long Yuan,[ab] Zhongyuan Liu,[a] Qiao Wang,[a] Keke Huang[a] and Shouhua Feng *[a]

Received 27th May 2019,
Accepted 17th July 2019

DOI: 10.1039/c9qm00346k

rsc.li/frontiers-materials

The general design strategy for excellent catalysts has been well established by the Sabatier principle, *e.g.*, moderate bond strength between the catalyst surface and the reactant/product. From the viewpoint of reaction kinetics, it is possible to modify the rate determining step through separately accelerating the adsorption and dissociation of intermediate products. In this research, we have demonstrated that OER kinetics for RuO_2 could be effectively promoted with the precise control of the reaction kinetics by optimizing the equilibrium of dissociation and recombination of water molecules. It is found that increasing the concentration of OH^- in the electrolyte contributes to the formation process of the peroxy species, Ru–OOH*, while the increase of temperature is helpful for the deprotonation process from a stabilized configuration of the peroxy species. With faster rate determining steps, RuO_2 shows excellent OER activity and stability under high temperature and concentrated basic electrolyte conditions. It is meaningful for accelerating the practical application of hydrogen production from electrolysis of water. And this research will provide a new perspective for the study of catalytic reactions, not just limited to the OER.

Introduction

Large scale storage of renewable energy produced by intermittent sources (such as solar and wind) is one of the most challenging research topics. Storing electrical energy in chemical bonds (H_2) by water electrolysis is an effective way to manipulate these clean energies.[1–4] This process consists of two half-reactions, *e.g.* hydrogen produced at the cathode and the oxygen evolution reaction (OER) at the anode. The OER involves a proton coupled four-electron transfer step.[5,6] It could only occur far from the equilibrium potential (1.23 V *vs.* RHE). This is the key factor causing the large efficiency loss during the overall water splitting reaction.[7,8] The sluggish OER kinetics has been attributed to the unfavorable formation energy of the peroxy species, M–OOH* (M represents the transition metal cation).[9–11] Moreover, this peroxy intermediate has been regarded as the precursor for the OER. Through adjusting the surface-oxygen adsorption energy, great progress has been made in facilitating the peroxy species formation. However, the reason why it needs an additional overpotential to drive the oxygen evolution after the formation of peroxy species (oxidation peak for M–OOH* in linear sweep voltammetry curve) is still a mystery.

A previous study has proved that the active oxygen species M–OOH* could stably exist on the surface of oxides.[12] It exactly explains why the OER needs an additional overpotential. Recently, combining the potential-dependent DFT calculation of the surface structure and *in situ* surface X-ray scattering, Shao-Horn *et al.* proposed a new OER pathway.[13] They found that the final proton release from a stabilized M–OOH* configuration is the rate determining step for the OER. This is because the peroxy species could be stabilized by a neighboring adsorbed group through a hydrogen bond.

Several efforts have been devoted to understanding the mechanisms and parameters that govern the oxygen evolution reaction process. According to the Sabatier principle, the best OER catalysts exhibit a medial surface–oxygen interaction, *e.g.* neither too weak (for peroxy species formation) nor too strong (for peroxy species dissociation).[14] Based on the molecular orbital theory, Shao-Horn *et al.* proposed a general design principle for OER catalysts: transition metal oxides with e_g filling slightly more than 1 show the best OER catalytic activity.[15,16] In addition, it has been proved that high activity and stability towards the OER can be realized with the O p-band centre position neither too close nor too far from the Fermi level.[17] This is because the O p-band centre

[a] *State Key Laboratory of Inorganic Synthesis and Preparative Chemistry, College of Chemistry, Jilin University, Changchun 130012, P. R. China. E-mail: shfeng@jlu.edu.cn*
[b] *Key Laboratory of Functional Materials Physics and Chemistry of the Ministry of Education, Jilin Normal University, Changchun 130103, P. R. China*

† Electronic supplementary information (ESI) available: Temperature/pH dependent Tafel curves and electrochemical impedance spectroscopy. See DOI: 10.1039/c9qm00346k

relative to the Fermi level of transition metal oxides scales linearly with the oxygen surface exchange kinetics.[18] Although these descriptors play a strong role in the prediction and design of excellent OER catalysts, they were all established based on the equilibrium between the adsorption and dissociation of intermediate products. Inevitably, it will sacrifice the advantage in reaction kinetics during an alternative process (adsorption or dissociation).

The rational design of catalysts is not the only way to achieve high catalytic activity. From the viewpoint of a reaction process, it is possible to modify the reaction kinetics through separately accelerating the adsorption and dissociation of intermediate products. These steps could be easily promoted by changing the reaction conditions. However, so far, this factor has been rarely explored in the research of catalytic OER. Herein, the effect of the reaction temperature and pH value on OER kinetics is systematically studied. As the best commercialized catalyst, RuO_2 is selected for the study. In order to adapt to the conditions of practical application, the temperature range is set as 0–75 °C which could be easily achieved in winter or under solar irradiance in summer. And the concentration of KOH is set as 0.1–5 M. With increasing pH, the Ru–OOH* formation is effectively accelerated. And with increasing temperature, the additional overpotential for deprotonation of the active oxygen species M–OOH* could be gradually eliminated. Because the decomposition of the peroxy species is accelerated, the stability of RuO_2 could be greatly promoted. Therefore, this research will provide a new perspective for the research of catalytic OER. It will further promote the practical application of the OER in large scale storage of renewable energy.

Experimental section

Polished glassy-carbon electrodes with a diameter of 5 mm were used as the working electrode. Acetylene black treated with nitric acid was used as the conductive agent and was mixed with oxide catalysts at a mass ratio of 5 : 1. An appropriate amount of neutralized Nafion (5% weight) was added into the catalyst ink.[15] The electrode had a final composition of 250 $\mu g_{oxide}\ cm_{disk}^{-2}$, 50 $\mu g_{AB}\ cm_{disk}^{-2}$, and 50 $\mu g_{Nafion}\ cm_{disk}^{-2}$.

To study the temperature dependence of the overpotential, electrochemical measurements were conducted in 0.1 M KOH electrolyte bubbled with O_2. All potentials are reported *versus* the reversible hydrogen electrode (RHE). It could be calculated according to the following equation:

$$E_{RHE} = E_{Hg/HgO} + E^{\theta}_{Hg/HgO} + \frac{RT}{nF}\ln\frac{p(H_2)}{a_{H^+}} + \Delta T \cdot E_T$$

where $E_{Hg/HgO}$ is the potential applied experimentally, $E^{\theta}_{Hg/HgO}$ is the standerd potential of the reference electrode *versus* the normal hydrogen electrode (0.098 V for Hg/HgO), R is the gas constant (8.314 J mol^{-1} K^{-1}), T is the temperature of the electrolyte, n is the number of transferred electron, F is the Faraday constant (96 485 C mol^{-1}), p is the hydrogen partial pressure, a is the activity of H^+, and E_T is the temperature coefficient for the Hg/HgO reference electrode (−0.001125 V $°C^{-1}$).[19] ΔT is the temperature difference from 25 °C for the test: $\Delta T = T_{Test} - 25$ (°C). With increasing temperature, the changes in the ion product of water were also studied and the constants are $\sim 10^{-14.94}$, $10^{-14.00}$, $10^{-13.27}$, and $10^{-12.71}$ from 0 to 75 °C.[20]

Linear voltammetric scanning (LSV) at a scan rate of 5 mV s^{-1} from −0.2 V to 0.9 V was used to study the oxygen evolution reaction on a CHI 660E electrochemical workstation in a three-electrode system (working electrode: rotating disk electrode coverd with oxides, reference electrode: Hg/HgO, counter electrode: platinum). Specific OER activity was obtained by normalizing the kinetic current with the surface area of the working electrode. Resistance compensation was accomplished with fitting series resistance by electrochemical impedance spectroscopy at high frequencies.

The faradaic efficiency was obtained with the rotating ring disk electrode method. And 0.4 V *vs.* RHE was applied to the Pt ring to reduce O_2 production.

For stability tests, *I*–*t* measurement was conducted at a specific potential with a current density of 10 mA cm^{-2}. In order to figure out the mechanism of property degradation, cyclic voltammetry was also performed from −0.2 V to *E*@10 mA cm^{-2} to obtain the stability data. After 1, 100, 500, and 1000 cycles, LSV was measured.

Results and discussion

The OER performance as a function of temperature (from 0 °C to 75 °C) was obtained through a drop coating method,[21] as shown in Fig. 1. Changes in temperature and the ion product of water were included during the potential correction for the reference electrode (as shown in Experimental section). Under standard conditions, the intrinsic OER catalytic activity of RuO_2 is similar to previously reported data in 0.1 M KOH at 25 °C,[22] *e.g.* with an overpotential (E_η@10 mA cm^{-2}) of ∼300 mV at an OER current density of 10 mA cm^{-2}. Interestingly, RuO_2 shows an enhanced OER performance as the temperature of the electrolyte monotonically increases. The E_η is dependent on temperature with a slope of −2.2 mV $°C^{-1}$. And the overpotential makes notable improvement at higher reaction temperatures (∼190 mV at 75 °C). Such a vast enhancement makes the activation of the oxygen evolution reaction very sensitive to changes in temperature.

To quantify this temperature dependence, we will focus on the potential at the oxidation peak ($E_{O–O}$) for the formation of peroxides and the onset OER potential (E_{OER}) for deprotonation of peroxides, which corresponds to the potential with a reaction current larger than the baseline current. It can be found that both $E_{O–O}$ and E_{OER} follow the same temperature direction. According to the literature, the oxidation peaks at ∼1.45 V belong to the formation of the active oxygen species, Ru–OOH*, from a Ru–OH* intermediate.[23] It was regarded as the rate determing step during the oxygen evolution reaction. With increasing temperature of the electrolyte, the potentials for Ru–OOH* formation ($E_{O–O}$) slightly decrease. And it shows a linear decrease with a slope of −0.21 mV $°C^{-1}$. Compared with $E_{O–O}$, the onset potentials for the OER (E_{OER}) decrease much more rapidly, with a slope of −1.09 mV $°C^{-1}$. Because the E_{OER}

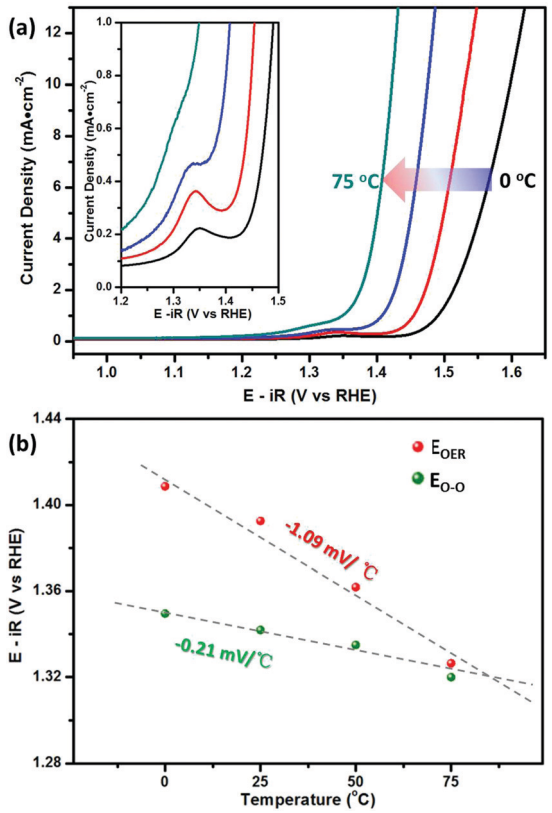

Fig. 1 OER performance in 0.1 M KOH for RuO_2 at different temperatures, ranging from 0 to 75 °C. (a) LSV curve; (b) temperature dependence of peroxy species formation (E_{O-O}) and deprotonation (E_{OER}).

decreases much more rapidly than E_{O-O}, the vast enhancement in OER performance at higher temperature mainly results from the lower overpotential in E_{OER}, rather than E_{O-O}.

In the Arrhenius equation $k = Ae^{-E_a/RT}$, E_a is the reaction activation energy which is a temperature independent constant. So, the reaction rate constant k will be increased with the reaction temperature. Generally, the OER current is proportional to the reaction rate of the RDS. The reaction rate can be evaluated by the charge transfer resistance between catalysts and the electrolyte. Electrochemical impedance spectra at $E@j$ = 10 mA cm^{-2} are shown in Fig. S1 (ESI†). It can be found that even with the same reaction rate (j = 10 mA cm^{-2}), the charge transfer resistance could be effectively reduced with increasing temperature. This indicates that a higher temperature will contribute to a faster kinetics. So, it will lead to the vast promotion of E_{OER}.

The difference in the Tafel slope has always been attributed to the different reaction barrier for the rate-determining step.[24] The distinct elementary process for the rate-determining step can be supposed from the value of Tafel slope. As shown in Fig. S2 (ESI†), the Tafel slope for RuO_2 gradually decreases from 110 mV dec^{-1} at 0 °C to 64 mV dec^{-1} at 75 °C. This indicates that the temperature of the electrolyte could induce significant changes in the reaction barrier of the RDS. According to the literature, we think the increase in temperature of the electrolyte is beneficial to the deprotonation process from M–OOH*.

As far as temperature is concerned, ionic activity will increase linearly with temperature. Then, a higher activity of OH^- will make a contribution to the decrease in E_{O-O}. This is very similar to the pH dependent OER performance through the decoupled proton–electron transfer reaction reported by Shao-Horn *et al.*[25] Here, the effect of ionic strength on the OER performance is confirmed by adding supporting electrolytes into 0.1 M KOH. In order to reduce the ion category, only potassium salts are included in the study (KCl and KNO_3). As shown in Fig. S3 (ESI†), the increase in ionic strength will decrease the ionic activity of OH^-, namely, a smaller effective concentration for OH^-. Then, the overpotentials for both mixing solutions increase obviously. So, the slight changes in E_{O-O} may result from the increase in the activity coefficient of OH^- at higher temperature for dilute alkaline solution (0.1 M KOH).

In order to evaluate the effect of ionic activity, pH dependent OER performance is shown in Fig. 2. It could be found that overpotentials at a current density of 10 mA cm^{-2} could be greatly reduced *via* increasing the electrolyte pH value. Compared

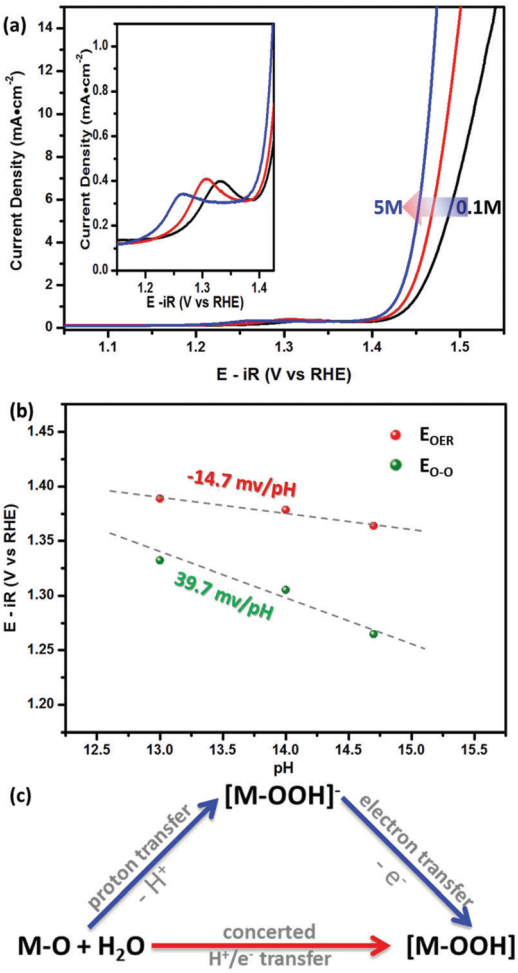

Fig. 2 OER performance of RuO_2 in different concentrations of KOH: 0.1 M, 1 M, and 5 M. (a) LSV curve; (b) pH dependence of peroxy species formation E_{O-O} and deprotonation E_{OER}; (c) reaction scheme for OH^- adsorption through a sequential or concerted proton-coupled electron transfer process.

with the overpotential in 0.1 M KOH electrolyte, E_η in 5 M KOH electrolyte could be significantly decreased by 51 mV. Such a vast enhancement must be correlated with the surface adsorption/desorption process for the intermediate products. To quantify the pH dependence, the pH dependence of (E_{O-O}) and (E_{OER}) is shown in Fig. 2(b). Different from the temperature dependence, we found that the E_{O-O} decreases much more rapidly than E_{OER} with increasing pH. And this linear relationship is different from the Nernst shift (with a slope of 59 mV per pH).[26] It has been explained by the decoupled proton–electron transfer reaction process during the formation of the active oxygen species.[27] So, it can be concluded that pH will make more contribution to the decrease in E_{O-O}.

A previous study has proved that the adsorption energy changes linearly with pH.[28] In the electrolyte with a higher pH value, water dipoles could stabilize the configuration of surface-adsorption. And it will result in a stronger adsorption.[29,30] Then, the anomalous pH dependent shift in RuO_2 electrochemical features is explained by a decoupled proton–electron transfer reaction process during the formation of the active oxygen species. Generally, the OER is realized through a proton-coupled electron transfer process, where the proton and electron are transferred simultaneously. It will prevent the formation of charged reaction intermediates which are usually high in energy. However, under a condition far from the neutral electrolyte, the transition metal oxide catalysts could sustain some degree of charge buildup accommodated by a change in the oxidation state. Then, the decoupled proton–electron transfer process can take place. As shown in Fig. 2c for M–OOH* formation, the proton and electron can transfer sequentially through a charged intermediate. Here, only the first step of M–OOH* formation under basic conditions is considered: $M–O_{ads} + OH^- \rightarrow M–OOH^-$. We apply a first-order rate-law approximation for this elementary reaction. Thus, the rate constant $k = k^\circ[OH^-][M–O_{ads}]$. So, the kinetic rate will increase linearly with the concentration of OH^-. This exactly explains the shift in E_{O-O}.

However, the difference in rate constant could only lead to changes in E_{O-O}. It cannot modify the deprotonation process from M–OOH* and could therefore play a negligible role in promoting E_{OER}. Most often, deprotonation is associated with the acid dissociation constant K_a. When the pH $\gg$ pK_a, the spontaneous proton dissociation equilibrium of M–OOH* will occur. According to DFT calculations, the M–OO* intermediate is unstable in aqueous solution. It will spontaneously decompose and release the oxygen molecule.[31] So, the slight shift in E_{OER} is related to proton dissociation.

The Tafel slopes at different pH values are shown in Fig. S4 (ESI†). With increasing pH value, a sequential increase in Tafel slope could be found. One possible explanation of this observation is that the high ionic activity of OH^- could accelerate the formation speed of the active oxygen species. It results from the decoupled proton–electron transfer process. Undoubtedly, a higher concentration of the reactant will accelerate the reaction rate. So a smaller reaction barrier would be needed to form the Ru–O–OH* precursor, by deprotonation of the Ru–OH* intermediate. Thus, the overpotential (E_η) is reduced.

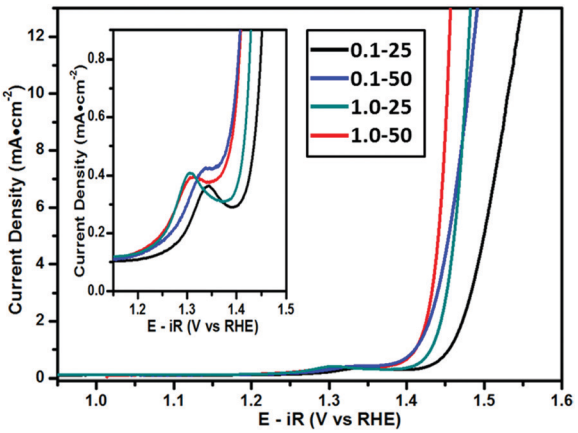

Fig. 3 Dependence of OER performance on temperature and pH under different reaction conditions.

Here, we can draw a preliminary conclusion, *i.e.*, high pH will contribute to decrease the E_{O-O}, while high temperature will contribute to lower the E_{OER}. Then, we check this rule by the OER in electrolytes at a high temperature (50 °C) and with a high pH (1.0 M KOH).

With the comparison of OER performance at 25 °C and 50 °C in 1.0 M KOH (olive green and red lines in Fig. 3), negligible changes in E_{O-O} could be found with the difference in temperature. As might have been expected, E_{OER} shows an obvious promotion. So, the decrease in overpotential must result from the enhancement of E_{OER}. This is because the same pH will lead to equal amounts of active peroxy species on the surface. Then the high temperature will accelerate the deprotonation process.

With the comparison of OER performance in 0.1 M and 1 M KOH at 50 °C (blue and red lines in Fig. 3), no obvious changes in E_{OER} could be found with the change in pH. So, the decrease in overpotential must result from the enhancement of E_{O-O}. This is because a higher pH will lead to more amounts of active peroxy species on the surface. It will provide more precursors for oxygen evolution.

In order to confirm that the reaction current truly results from oxygen evolution rather than side reactions, the OER faradaic efficiency (FE) is investigated by the rotating ring-disk electrode (RRDE) method.[32] With a high rotating... speed of 1600 rpm, oxygen from the centre of the RRDE electrode could be reduced again to OH^- around the Pt ring. As shown is Fig. S5 (ESI†), even under high temperature and high pH conditions, the FE for oxygen evolution could remain over 94%.

Based on the experiment in this paper, we have found that a higher pH value of the electrolyte is helpful for the promotion of the 2nd step (Fig. 4(a)) through modification of the adsorption energy. After that, a stable configuration of the peroxy species Ru–OOH* will be formed through a hydrogen bond with the neighbouring –OH group. Most importantly, we also find that a higher temperature of the electrolyte will make a contribution to the subsequent deprotonation step. Then, a vast enhancement of the OER performance could be easily realized under unconventional conditions. Compared with the standard condition (25 °C, 0.1 M KOH), the overpotential (50 °C, 1.0 M KOH) is decreased by 80 mV

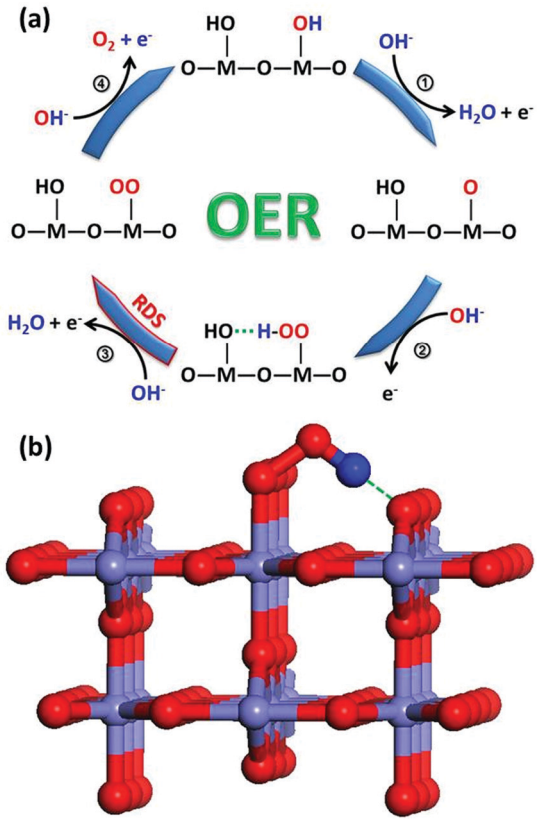

Fig. 4 (a) OER mechanism on transition-metal oxide catalysts *via* 4 electron transfer steps. (b) Stable configuration for the peroxy species through a hydrogen bond.

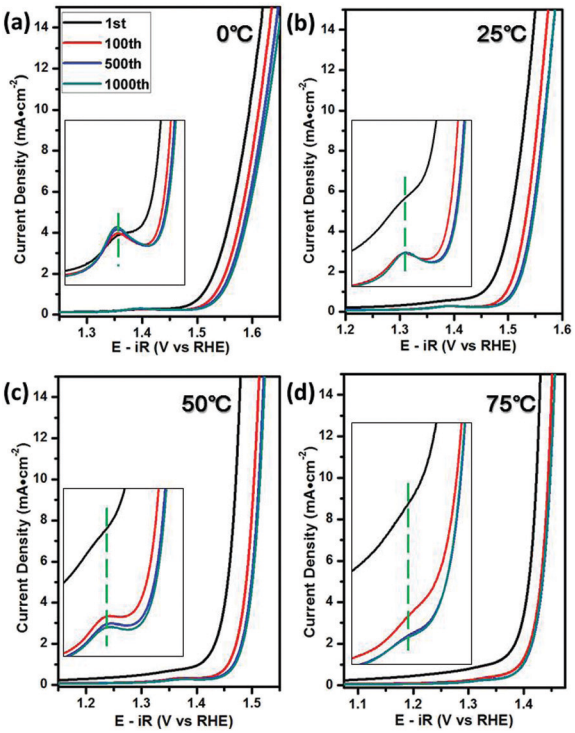

Fig. 5 OER stability tests through the CV method under 0.1 M KOH at different temperatures: (a) 0 °C; (b) 25 °C; (c) 50 °C; and (d) 75 °C.

for RuO_2, as shown in Fig. 3. Due to the decrease in efficiency loss, such vast enhancement will be significant for practical applications.

Since the OER performance could be enhanced under unconventional conditions (high temperature and high OH^- concentration), the stability of the catalyst should be taken into consideration for commercial applications. Here, the electrochemical durability of RuO_2 powders is evaluated by repeating the CV cycles. As shown in Fig. 5, RuO_2 shows excellent stability at higher temperature. And the increase in overpotential (10 mA cm^{-2}) is gradually reduced from 38 mV (0 °C) to 26 mV (75 °C). From the insets, it can be found that the oxidation peaks for the formation of the Ru–OOH* species are enlarged after the CV measurement, especially at higher temperatures. This indicates that the number of active sites is increased.[33] This phenomenon may result from a surface reconstruction of the catalysts which will be helpful in exposing the active sites (coordinatively unsaturated Ru sites).

Due to the invisible changes in the potentials for the formation of the M–OOH* precursor, the stability must be restricted by the E_{OER}. So the decrease in catalytic activity is mainly derived from the unfavourable E_{OER}. It might have resulted from the abundant –OH or –OOH dipoles on the surface. A complex hydrogen bonded configuration will result in a higher stability of the peroxy species. It must lead to a higher overpotential of the deprotonation process. Since the high temperature could make a contribution to lower the E_{OER}, RuO_2 therefore shows an enhanced stability performance at higher temperature.

The effect of OH^- activity (pH) on its stability is also evaluated by the same method. The increase in overpotential (10 mA cm^{-2}) is gradually reduced from 38 mV (0.1 M KOH) to 18 mV (5 M KOH). The oxidation peak intensity for M–OOH* formation shows an moderate increase with increasing OH^- concentration, especially in concentrated alkali solution (high pH). This indicates that the number of active sites is also increased. Since the formation of the M–OOH* precursor is the guarantee for stability, it is reasonable to draw the conclusion that a higher concentration of OH^- could accelerate the formation process and therefore make a contribution to the stability, as shown in Fig. 6.

Since the temperature and pH value of the electrolyte are the two key factors for the promotion for E_{O-O} and E_{OER} separately, the combination of high temperature and high pH value ensures a large increase in stability. Compared with standard conditions, a substantial increase in stability is obtained under extreme conditions (75 °C, 5.0 M concentrated alkali solution). Even after 1000 CV cycles, the overpotential increases by only 11 mV. In addition, catalyst durability under OER conditions was studied with *I–t* measurement at a specific potential with a current density of 10 mA cm^{-2}. As shown in Fig. 6(e), high temperature and concentrated bases are good for retaining the catalyst stability. After 12 h, the current density could still remain over 90%, while it could only remain at 35% in 0.1 M KOH at 25 °C.

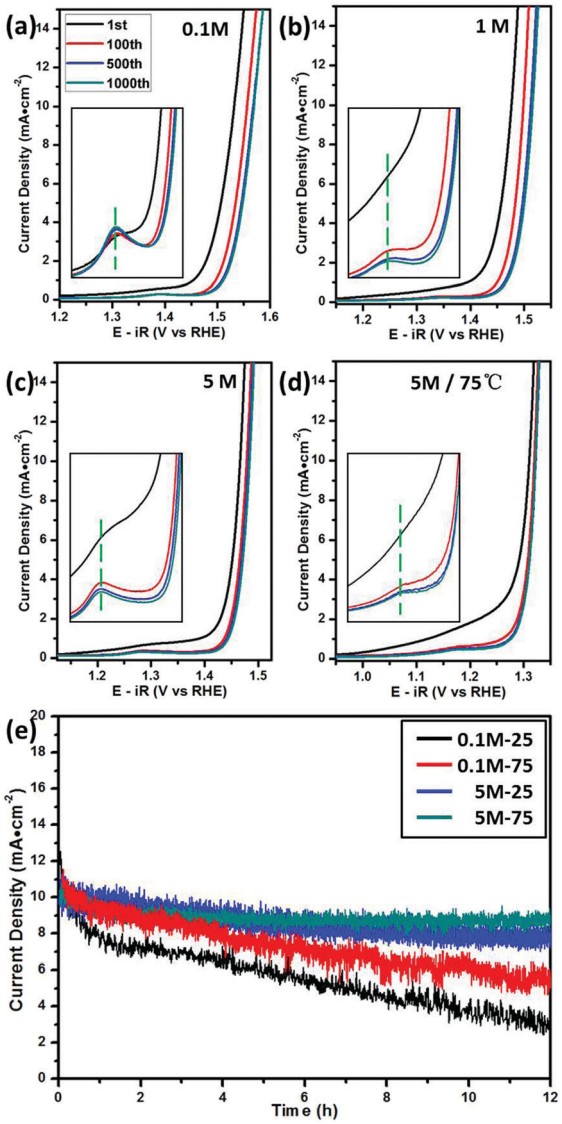

Fig. 6 OER stability tests through the CV method at 25 °C with different concentrations of KOH: (a) 0.1 M; (b) 1.0 M; (c) 5.0 M and (d) extreme condition: 5.0 M and 75 °C. (e) *I*–*t* curves under different OER conditions.

Conclusions

In summary, OER performances of RuO_2 powders were studied under unconventional conditions (high temperature and concentrated base). It was proved that the activity of OH^- determined the first RDS in the OER, namely, the formation of peroxy species M–OOH*, while the temperature of the electrolyte controlled the second RDS in the OER, *e.g.* deprotonation of the peroxy species. With precise control of the reaction conditions, the adsorption and dissociation equilibrium of the peroxy species could be easily realized. With the assistance of high temperature and high OH^- activity, RuO_2 exhibited an excellent OER catalytic performance, much better than that under standard conditions. Due to the acceleration in kinetics of RDSs, a remarkable enhancement of stability was also realized. Therefore, this research will provide an effective method for the enhancement of OER performance.

Conflicts of interest

There are no conflicts to declare.

Acknowledgements

This work was supported by the China Postdoctoral Science Foundation (2018M641773) and the National Natural Science Foundation of China (21801089, 21671076, 21427802).

References

1 J. Hwang, R. R. Rao, L. Giordano, Y. Katayama, Y. Yu and Y. Shao-Horn, *Science*, 2017, **358**(6364), 751–756.
2 T. R. Cook, D. K. Dogutan, S. Y. Reece, Y. Surendranath, T. S. Teets and D. G. Nocera, *Chem. Rev.*, 2010, **110**, 6474–6502.
3 N. T. Suen, S. F. Hung, Q. Quan, N. Zhang, Y. J. Xu and H. M. Chen, *Chem. Soc. Rev.*, 2017, **46**, 337–365.
4 M. Tahir, L. Pan, F. Idrees, X. Zhang, L. Wang, J. Zou and Z. L. Wang, *Nano Energy*, 2017, **37**, 136–157.
5 L. Giordano, B. Han, M. Risch, W. T. Hong, R. R. Rao, K. A. Stoerzinger and Y. Shao-Horn, *Catal. Today*, 2016, **262**, 2–10.
6 J. M. Mayer, *Annu. Rev. Phys. Chem.*, 2004, **55**, 363–390.
7 L. Duan, F. Bozoglian, S. Mandal, B. Stewart, T. Privalov, A. Llobet and L. Sun, *Nat. Chem.*, 2012, **4**(5), 418–423.
8 C. C. L. McCrory, S. Jung, J. C. Peters and T. F. Jaramilo, *J. Am. Chem. Soc.*, 2013, **135**(45), 16977–16987.
9 B. J. Trzesniewski, O. Diaz-Morales, D. A. Vemaas, A. Longo, W. Bras, M. T. M. Koper and W. A. Smith, *J. Am. Chem. Soc.*, 2015, **137**, 15112–15121.
10 H. Y. Wang, S. F. Hung, Y. Y. Hsu, L. Zhang, J. Miao, T. S. Chan, Q. Xiong and B. Liu, *J. Phys. Chem. Lett.*, 2016, **7**, 4847–4853.
11 J. Chen and A. Selloni, *J. Phys. Chem. Lett.*, 2012, **3**, 2808–2814.
12 O. Diaz-Morales, D. Ferrus-Suspedra and M. T. M. Koper, *Chem. Sci.*, 2016, **7**, 2639–2645.
13 R. R. Rao, M. J. Kolb, N. B. Halck, A. F. Pedersen, A. Mehta, H. You, K. A. Stoerzinger, Z. Feng, H. A. Hansen, H. Zhou, L. Giordano, J. Rosmeisl, T. Vegge, I. Chorkendorff, I. Stephens and Y. Shao-Horn, *Energy Environ. Sci.*, 2017, **10**, 2626–2637.
14 J. Greeley, I. E. Stephens, A. S. Bondarenko, T. P. Johansson, H. A. Hansen, T. F. Jaramillo, J. Rossmeisl, I. Chorkendorff and J. K. Norskov, *Nat. Chem.*, 2009, **1**, 552–556.
15 J. Suntivich, K. J. May, H. A. Gasteiger, J. B. Goodenough and Y. Shao-Horn, *Science*, 2011, **334**, 1383–1385.
16 C. Wei, Z. Feng, G. G. Scherer, J. Barber, Y. Shao-Horn and Z. J. Xu, *Adv. Mater.*, 2017, **29**, 1606800.
17 W. T. Hong, M. Risch, K. A. Stoerzinger, A. Grimaud, J. Suntivich and Y. Shao-Horn, *Energy Environ. Sci.*, 2015, **8**(5), 1404–1427.
18 A. Gupta, W. D. Chemelewski, C. Buddie Mullins and J. B. Goodenough, *Adv. Mater.*, 2015, **27**(39), 6063–6067.
19 J. Suntivich, H. A. Gasteiger, N. Yabuuchi, H. Nakanishi, J. B. Goodenough and Y. Shao-Horn, *Nat. Chem.*, 2011, **3**(7), 546–550.
20 S. G. Bratsch, *J. Phys. Chem. Ref. Data*, 1989, **18**(1), 1–21.

21 W. L. Marshall and E. U. Franck, *J. Phys. Chem. Ref. Data*, 1981, **10**(2), 295–304.
22 L. C. Seitz, C. F. Dickens, K. Nishio, Y. Hikita, J. Montoya, A. Doyle, C. Kirk, A. Vojvodic, H. Y. Hwang, J. K. Norskov and T. F. Jaramollo, *Science*, 2016, **353**(6303), 1011–1014.
23 T. Reier, M. Oezaslan and P. Strasser, *ACS Catal.*, 2012, **2**, 1765–1772.
24 D. K. Bediako, Y. Surendranat and D. G. Nocera, *J. Am. Chem. Soc.*, 2013, **135**, 3662–3674.
25 K. A. Stoerzinger, R. R. Rao, X. R. Wang, W. T. Hong, C. M. Rouleau and Y. Shao-Horn, *Chem*, 2017, **2**, 668–675.
26 C. Liu, D. Bocchicchio, P. Overmyer and M. Neuman, *Science*, 1980, **207**, 188–189.
27 M. E. Lyons and S. Floquet, *Phys. Chem. Chem. Phys.*, 2011, **13**, 5314–5335.
28 D. Y. Kuo, J. K. Kawasaki, J. N. Nelson, J. Kloppenburg, G. Hautier, K. M. Shen, D. G. Schlom and J. Suntivich, *J. Am. Chem. Soc.*, 2017, **139**, 3473–3479.
29 M. H. Hansen and J. Rossmeisl, *J. Phys. Chem. C*, 2016, **120**(51), 29135–29143.
30 E. Watanabe, J. Rossmeisl, M. E. Bjorketun, H. Ushiyama and K. Yamashita, *J. Phys. Chem. C*, 2016, **120**(15), 8096–8103.
31 M. H. Seo, H. W. Park, D. U. Lee, M. G. Park and Z. Chen, *ACS Catal.*, 2015, **5**, 4337–4344.
32 S. Zhao, Y. Wang, J. Dong, C. T. He, H. Y. P. An, K. Zhao, X. Zhang, C. Gao, L. Zhang, J. Lv, J. Wang, J. Zhang, A. M. Khattak, N. A. Khan, Z. Wei, J. Zhang, S. Liu, H. Zhao and Z. Tang, *Nat. Energy*, 2016, **1**(12), 16184.
33 K. A. Stoerzinger, L. Qiao, M. D. Biegalski and Y. Shao-Horn, *J. Phys. Chem. Lett.*, 2014, **5**, 1636–1641.